Seismological Research Letters

A Single Bit Matters: Coherent Noise of Seismic Data Loggers

by Ryota Takagi, Kiwamu Nishida, Yosuke Aoki, Takuto Maeda, Komei Masuda, Minoru Takeo, Kazushige Obara, Katsuhiko Shiomi, Minemori Sato, and Kazuo Saito

INTRODUCTION

Cross-correlating seismic random signals, such as coda waves or ambient noise, at two sites can extract seismic wavefields as if a source is at one site and a receiver is at the other if certain conditions are met (e.g., Aki, 1957; Campillo and Paul, 2003). Given the recent development of dense seismic network, the last decade has witnessed the rapid emergence of imaging Earth's local (Nagaoka *et al.*, 2012), regional (Shapiro *et al.*, 2005; Nishida *et al.*, 2008; Lin *et al.*, 2011), and global (Nishida *et al.*, 2009) seismic structures and their temporal changes (Brenguier, Campillo, *et al.*, 2008; Brenguier, Shapiro, *et al.*, 2008; Nagaoka *et al.*, 2010; Brenguier *et al.*, 2014) from these random signals.

With this trend of research, we fortuitously found peculiar pulses in the cross correlations of the Japanese high-sensitivity seismograph network (Hi-net; Obara *et al.*, 2005) seismic records (Fig. 1). Here, we used one-month records for January 2012 at 142 Hi-net stations in southwest Japan. Applying a band-pass filter of 10–20 s to correlograms reveals sharp pulses at lag times of every 60 s (Fig. 1a). Unfiltered correlograms nicely demonstrate a propagation of Rayleigh waves, but a closer look at locations where no wavetrain is extracted reveals sharp pulses at lag times of every second (Fig. 1b).

These regular pulses obviously do not reflect the internal structure of the Earth, but instead are of electronic origin within a data acquisition system. We explore the causes of these pulses using various datasets. First, we briefly overview the system of seismic data acquisition. Then we check whether these pulses exist in observed seismograms, as well as the correlograms, and explore the origin of these pulses by changing configurations of the data loggers. Finally, we give some caveats to performing cross correlations of ambient seismic noise to get rid of these artificial pulses.

DATA ACQUISITION SYSTEM

Figure 2 schematically depicts a typical acquisition system of digital seismic data. A velocity seismometer outputs voltage that is converted from the velocity of the sensor by a relationship prescribed for each sensor. A data logger converts the voltage to quantized digits by an internal analog–digital converter.

We obtain digital velocity records by converting the quantized digits to velocity by the relationships of the velocity and the voltage and of the analog voltage and the quantized digits.

In seismic observations, calibrating precise timing is important. Modern seismic acquisition calibrates time by synchronizing an internal clock of a data logger with a Global Postioning System (GPS) signal from an antenna attached to the data logger (Fig. 2). The frequency of the time calibration is designed by each data logger (e.g., every second using pulse-per-second signals of GPS).

DATA ANALYSIS

First we checked whether the peculiar pulses exist in raw observed signals as well as correlograms. In Figure 3a and 3b, respectively, unfiltered seismograms are stacked every minute and second over a one-year period in 2013 of three-component signals of all Hi-net stations (about 780 stations). Note that vertical axes are in digits, not velocity. Because all Hi-net sites used the same data logger (Keisokugiken HKS-9200) in 2013, everything we see in Figure 3 does not come from the Earth, but from a mechanics of a data logger. Anything originating from the Earth disappears after an extensive stacking because it is obviously not precisely periodic in time.

Figure 3a shows pulses with heights of about one digit every second. Stacking the seismograms every second yields a distinct pulse at around 0.07 s (Fig. 3b), indicating that some processes repeating precisely every second in a data logger generate the pulses seen in Figure 3a. Figure 3a also shows a broader pulse at around 3 s, indicating the existence in a data logger of a processing repeating precisely every minute.

To explore the origin of these features and to verify that they are not specific to a particular data logger but are instead generic features, we conducted a test with a different data logger (Hakusan LS-7000XT) and connected a resistance of 10 kΩ, a typical coil resistance of electromagnetic seismometers, to the input of the logger. When the timing is calibrated every second, the time series stacked every minute over a one-day period yields sharp positive and negative pulses with heights of 0.3–0.4 digits (Fig. 4a). Stacking the same time series every second yields a positive pulse with a height of about 0.2 digits peaked at around 0.25 s and a negative offset at about 0.1
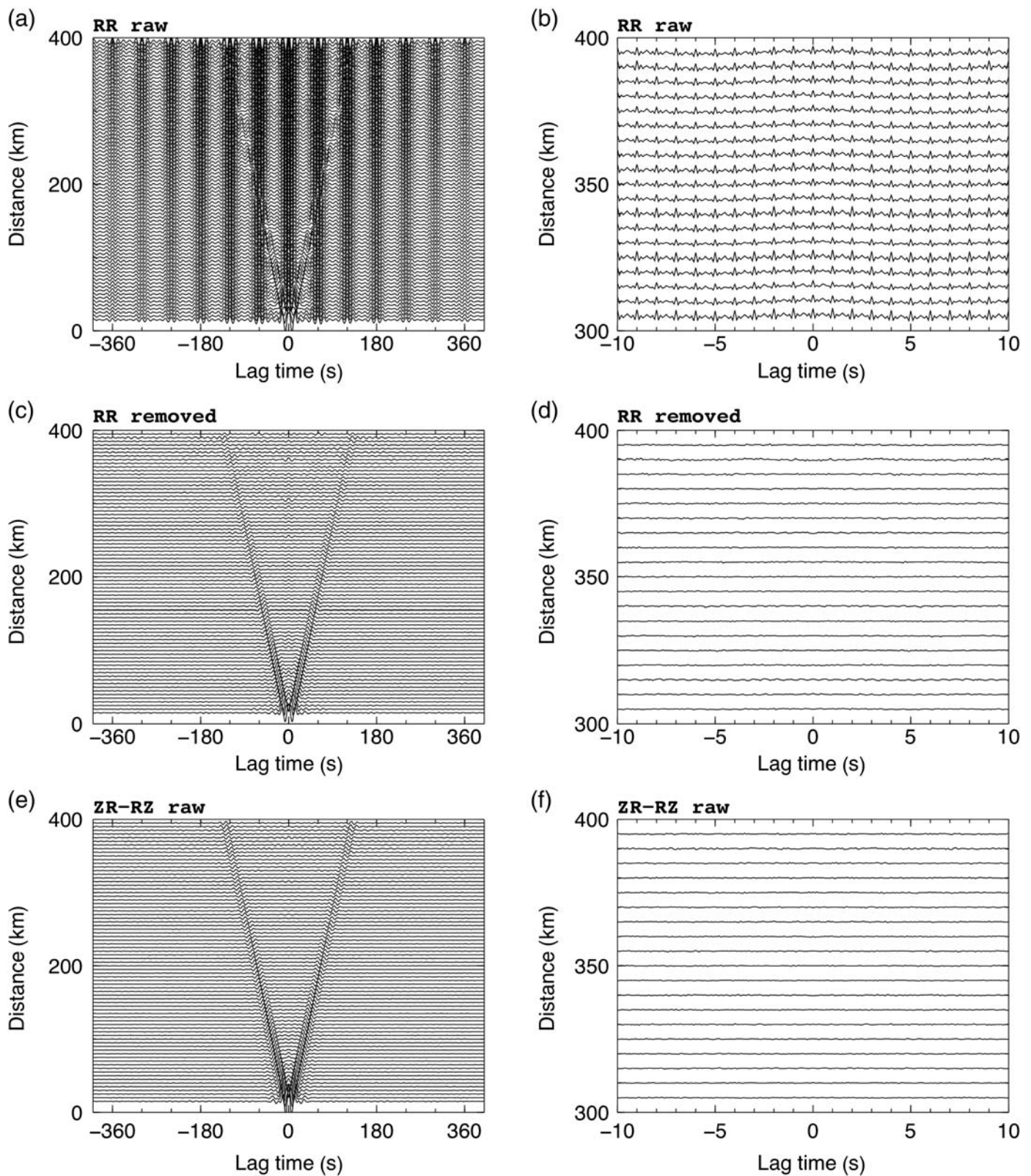
▲ **Figure 1.** Correlograms of ambient seismic noise aligned along the interstation distance. (a) Correlograms with a band-pass filter between 10 and 20 s. (b) Unfiltered correlograms of a portion where no extracted wave propagation is expected. (c,d) Same as (a) and (b) but the quantization errors are subtracted from the raw data before cross correlation. (e,f) Same as (a) and (b) but the difference of ZR and RZ correlations is taken without subtraction of the quantization error. The amplitude scales of (c,e) and (d,f) are the same as those of (a) and (b), respectively.
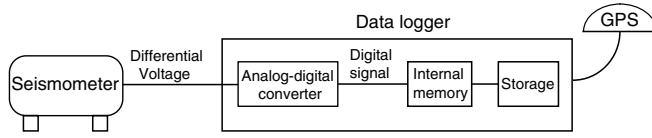
▲ **Figure 2.** A schematic representation of seismic data acquisition. A seismometer output differential voltage, which a data logger takes as an input. An analog–digital converter converts the voltage signal to digital signals, which are stored initially in an internal memory and finally in a data storage. The data are written to the storage by a prescribed interval, every minute, for example.
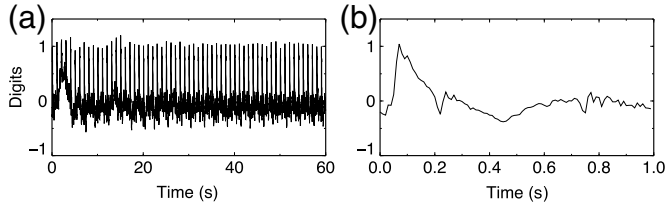
▲ **Figure 3.** Stacked seismograms of the three components of all Hi-net stations in 2013. (a) Seismograms with a stacking every minute. (b) Same as (a) except that the stacking is made every second.

▲ **Figure 4.** Stacked time series of the output from a one-day record with the Hakusan LS-7000XT data logger by connecting a resistance of 10 kΩ, a typical coil resistance of electromagnetic seismometers, for each component as input. (a) Time series stacked every minute, with time calibration every second. (b) Same as (a) but the stacking is made every second. (c,d) Same as (a) and (b) but the time calibration is every hour.
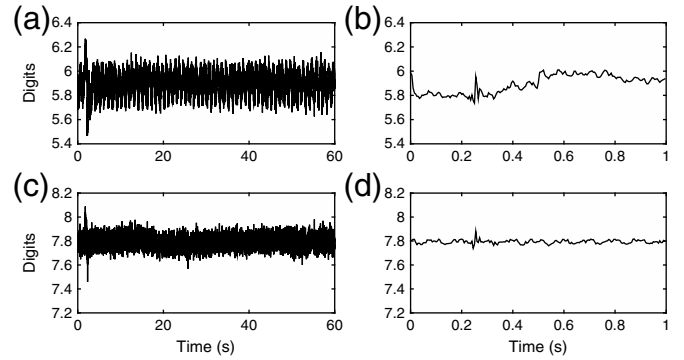
digits at around 0.5 s (Fig. 4b), implying a process repeating every second or its multiples.

To figure out the effect of time calibration, we conducted the same experiment by changing the interval of time calibration from every second to every hour. Stacked time series show that the pulses we saw in the previous experiment at around 0.25 s still remain with reduced amplitudes (Fig. 4c,d), but the offset at around 0.5 s disappears. This indicates that pulses repeating every second as seen in Figures 1b, 3, and 4b,d are partially due to time calibration.

Experiments discussed above (Fig. 4) were conducted by connecting resistances to the input. To understand the effect of the amplitude of input signals, we conducted the same experiment with a short circuit of the sensor input, keeping the time calibration interval of 1 hr. Overall amplitude of the pulses and offsets in this case is similar (Fig. 5), indicating that the dependence of the signal strength is not seen from our experiments.

GENERAL FEATURE OF THE PULSES

Our investigation revealed that perturbations in a data logger repeating every second and minute may be a ubiquitous feature in modern data loggers that deliver digital signals. Because all data loggers in this study are configured to write to the storage or transmit the data every minute, pulses every minute are likely to be related to them. These pulses emerge coherently over time and stations equipped with the same data logger. Thus, we refer to these pluses originating from data loggers to as "coherent logger noise."

Although the internal perturbations every second and minute are ubiquitous features, details differ among data loggers and situations of data acquisition. For example, the pulses every second are about 1 digit high in the Hi-net case with the Keisokugiken HKS-9200 (Fig. 3), whereas they are lower in experiments with the Hakusan LS-7000XT (Fig. 4). This difference implies that the input signals are processed differently in different data loggers or the amplitude of these pulses may depend on the amplitude of input signals.

Pulses at lag times every 60 s (Fig. 1a) are obtained because the Hi-net deploys seismometers with a natural frequency of 1 Hz, which do not have much sensitivity to oscillations with periods longer than 10 s. In other words, cross-correlating broadband seismograms do not require a care about these perturbations by a data logger. This can be understood by comparing the coherent logger noise with ambient seismic noise recorded by broadband seismometers.

COHERENT LOGGER NOISE

Because of the existence of the coherent logger noise, observed data at the ith station may be represented by $d_i = s_i + n_i + e_i$, in which d_i, s_i, n_i, and e_i are observed data, signals originating from, for example, earthquakes, or interaction between solid Earth, ocean, and atmosphere, incoherent noise originating from an uncorrelated fluctuation of the electronic current in a seismometer, and the coherent logger noise, respectively. In this case, the power spectrum of ith station is represented as

$$\langle d_i^* d_i \rangle = \langle s_i^* s_i \rangle + \langle n_i^* n_i \rangle + \langle e_i^* e_i \rangle, \tag{1}$$

and the cross spectrum between ith and jth stations is given by

$$\langle d_i^* d_j \rangle = \langle s_i^* s_j \rangle + \langle e_i^* e_j \rangle, \tag{2}$$
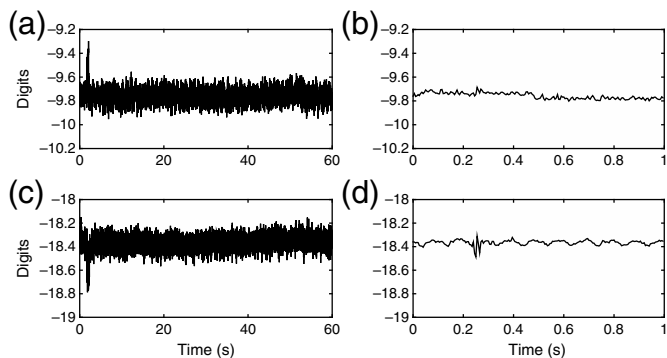
▲ **Figure 5.** Same as Figure 4, but the input is short circuited.

in which * denotes the complex conjugate and ⟨⟩ denotes time average. We assume $\langle n_i^* n_j \rangle = 0$ when $i \neq j$, and $\langle s_i^* n_j \rangle = 0$, $\langle s_i^* e_j \rangle = 0$, and $\langle n_i^* e_j \rangle = 0$. The magnitude relationship between $\langle s_i^* s_j \rangle$, $\langle n_i^* n_j \rangle$, and $\langle e_i^* e_j \rangle$ is a key to understanding how much the coherent logger noise affects the observed power and cross spectra.

To understand the magnitude relation, we examined the power spectra of the coherent logger noise and observed records at a short-period Hi-net station (JIZH) and broadband F-net station (JIZF) on a day with typical ambient noise level (10 January 2014). Because the Hi-net and F-net stations are separated by less than 100 m and installed in the same tunnel, we can assess the effect of different sensors on the observed power spectra of the Hi-net and F-net data. The power spectra are estimated from nine time windows, each of which has a length of 655.36 s with a 50% of overlapping with the next window, leading to a total length of data of 3256.8 s. We obtained the power spectra of the coherent logger noise shown in Figure 3a, after converting the quantized digits to particle velocity by the sensitivity of the digitizer, 5.87931×10^{-10} m/s/digit. For the Hi-net data and the coherent logger noise, we deconvolved the instrumental response of the short-period Hi-net sensor (Maeda *et al.*, 2011).

Figure 6 shows the power spectra of the coherent logger noise and of the Hi-net and F-net records. The power spectrum of the coherent logger noise has impulsive peaks at 1/60 Hz, 1 Hz, and those overtones. Because the coherent logger noise is completely periodic, the peaks get higher and narrower with the data length increasing. We should note that the integrated power of the coherent logger noise within frequency ranges has to be compared with those of Hi-net and F-net records. The power of Hi-net records is larger than that of the coherent logger noise by one order of magnitude or more. However, this does not mean that we can rule out the effect of the coherent logger noise in the cross spectrum. We should note the term of the incoherent noise $\langle n_i^* n_i \rangle$ in the power spectrum (equation 1) that does not emerge in the cross spectrum (equation 2). Because the short-period Hi-net sensor with a natural frequency of 1 Hz is less sensitive to low-frequency oscillations, the incoherent noise may largely contaminate the low-frequency component below 1 Hz.
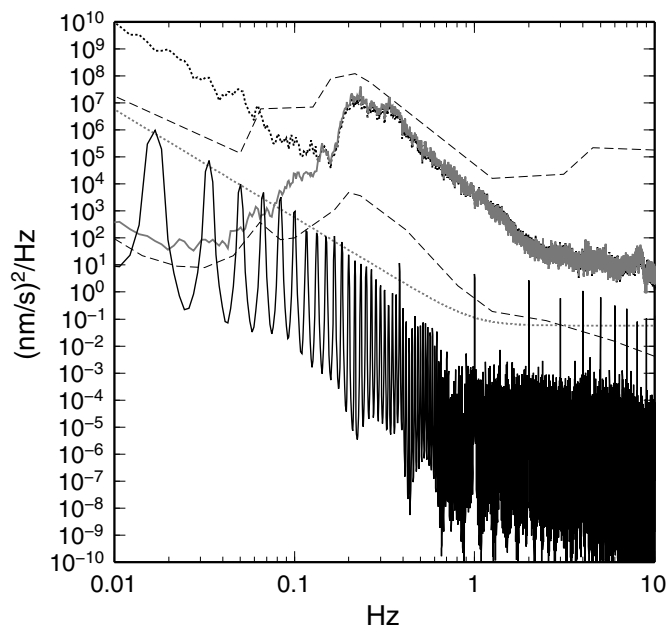
▲ **Figure 6.** Power spectra of the coherent logger noise (solid black line) and observed records at the collocated Hi-net (dotted black line) and F-net stations (gray line). The dotted gray line is the power spectrum of the quantization error, which is the minimum noise level due to the conversion from continuous analog to discrete digital data. We assume that the quantization error is random white noise distributing uniformly from 0 to 1 digit. The Hi-net record, the coherent logger noise, and the quantization error are deconvolved with the instrumental response of the short-period Hi-net sensor. The dashed black lines show the new low-noise model (NLNM) and the new high-noise model (NHNM) by Peterson (1993).

In contrast to Hi-net sensors, F-net is deployed with an STS-2 seismometer, which has a flat response up to 120 s. If we assume that the incoherent noise of the broadband F-net sensor and the coherent logger noise are much smaller than the signal amplitude, the power spectrum of the F-net record represents the contribution of the signals $\langle s_i^* s_i \rangle$ within the observed power spectrum of the short-period Hi-net sensor $\langle d_i^* d_i \rangle$. The difference between the power spectra of the Hi-net and the F-net records reflects the incoherent noise in the Hi-net sensor, $\langle n_i^* n_i \rangle$. Figure 6 shows the increase in the contribution of the incoherent noise below 0.2 Hz. At lower frequencies below 0.1 Hz, the power of the coherent logger noise gets larger than that of the F-net data, indicating that $\langle s_i^* s_i \rangle < \langle e_i^* e_i \rangle$. Accordingly, we should pay much attention to the coherent logger noise when we discuss cross correlations of short-period seismograms in frequency ranges below the natural frequency of a seismometer.

The cross spectrum $\langle s_i^* s_j \rangle$ that relates to the Green's function decays with separation distance because of geometrical spreading. Wave scattering and attenuation effect also decrease the amplitude of the cross spectrum, especially in high frequencies. On the other hand, the coherent logger noise is consistent

among all stations if they have the same data logger. Thus, the geometrical spreading, scattering, and attenuation effects may accelerate the dominance of the coherent logger noise in cross correlations.

REMEDY TO REMOVE COHERENT LOGGER NOISE

The amplitude of the coherent logger noise is only up to a few digits, much smaller than the seismic signal and incoherent noise, so it is invisible in the raw data. Analyses of earthquakes thus do not require care of the coherent logger noise. On the other hand, noise cross-correlation analyses reveal the tiny coherent logger noise by stacking the coherent portion in a large amount of data. Because we now know the characteristics of the coherent logger noise, we suggest two remedies to remove the coherent logger noise from cross-correlation functions of seismic ambient noise.

The first and more intuitive remedy is to subtract the coherent logger noise from the raw data and then to compute cross-correlation functions. The waveform of the coherent logger noise may be extracted by the stacking procedure discussed in the previous section. Here we subtracted the stacked waveform of all Hi-net stations shown in Figure 3a from each Hi-net record and then computed cross correlations. Figure 1c,d depicts the correlograms after the subtraction of the coherent logger noise, indicating that the period pulses due to the coherent logger noise are clearly reduced. More specifically, the coherent logger noise repeating every second is more effectively removed as compared with those repeating every minute. This first remedy can be applied to the cross-correlation analysis of all components and to other analyses. The effective subtraction extends the lower limit of frequency range with short-period sensors.

The second remedy is a method to take advantage of the nature of elliptic particle motions in Rayleigh waves, which have a 90° phase difference between vertical and radial motions. These characteristics result in the opposite sign of vertical–radial (ZR) and radial–vertical (RZ) cross correlations (Takagi *et al.*, 2014). In contrast, the coherent logger noise is equally appended to all components of seismic records without a phase difference so that ZR and RZ cross correlations exhibit the same sign. The difference between ZR and RZ cross correlations thus extracts propagating Rayleigh waves without the contamination of the coherent logger noise (Fig. 1e,f). This method neither requires the waveform of the coherent logger noise nor an assumption that the coherent logger noise is invariant of time and stations. This is an advantage of the second remedy as compared to the first remedy. The ZR and RZ cross correlations give more robust estimation of the Green's function even with a contamination of mechanical errors, not only from data with anisotropic source distribution (van Wijk *et al.*, 2011; Haney *et al.*, 2012). The theoretical basis of this remedy is described in the Appendix.

SUMMARY

We found coherent noise in seismic data loggers repeating every 1 and 60 s. Although both seismic data loggers (the Keisokugiken HKS-9200, which is deployed in the Hi-net sites, and the Hakusan LS-7000XT) generate the coherent noise repeating every 1 and 60 s, the detailed feature of the coherent noise depends on the data logger. A part of the coherent noise repeating every second occurs when the time calibration is made either every second or hour so that it is partially due to the time calibration. The coherent noise repeating every minute occurs ubiquitously, but the shape of the pulse is different in different data loggers. We suggest that the coherent noise repeating every minute arises when the system writes the data to its data storage.

The amplitude of the coherent logger noise is so tiny, with only up to a few digits, that it does not affect the waveform of earthquakes. However, it affects the waveform of the cross correlation of ambient noise, for example, with small amplitudes. In particular, the coherent logger noise shows the greatest effects when we try to explore signals of longer period from short-period seismometers.

We offer two remedies to get rid of the coherent logger noise from correlograms of ambient noise: (1) subtract the coherent logger noise from the raw data and then to compute cross-correlation functions, and (2) take advantages of the nature of elliptic particle motions in Rayleigh waves with a 90° phase difference between vertical and radial motions. We found both methods are effective in removing the coherent logger noise, but the second method works better. ◪

REFERENCES

Aki, K. (1957). Space and time spectra of stationary stochastic waves, with special reference to microtremors, *Bull. Earthq. Res. Inst. Univ. Tokyo* **25,** 415–457.

Brenguier, F., M. Campillo, C. Hadziioannou, N. M. Shapiro, R. M. Nadeau, and E. Larose (2008). Postseismic relaxation along the San Andreas fault at Parkfield from continuous seismological observations, *Science* **321,** 1478–1481, doi: 10.1126/science.1160943.

Brenguier, F., M. Campillo, T. Takeda, Y. Aoki, N. M. Shapiro, X. Briand, K. Emoto, and H. Miyake (2014). Mapping pressurized volcanic fluids from induced crustal seismic velocity drops, *Science* **345,** 80–82, doi: 10.1126/science.1254073.

Brenguier, F., N. M. Shapiro, M. Campillo, V. Ferrazzini, Z. Duputel, O. Coutant, and A. Nercessian (2008). Towards forecasting volcanic eruptions using seismic noise, *Nat. Geosci.* **1,** 126–130, doi: 10.1038/ngeo104.

Campillo, M., and A. Paul (2003). Long-range correlations in the diffuse seismic coda, *Science* **299,** 547–549, doi: 10.1126/science.1078551.

Haney, M. M., T. D. Mikesell, K. van Wijk, and H. Nakahara (2012). Extension of the spatial autocorrelation (SPAC) method to mixed-

component correlations of surface waves, *Geophys. J. Int.* **191,** 189–206, doi: 10.1111/j.1365-246X.2012.05597.x.

Lin, F.-C., M. H. Ritzwoller, Y. Yang, M. P. Moschetti, and M. J. Fouch (2011). Complex and variable crustal and uppermost mantle seismic anisotropy in the western United States, *Nat. Geosci.* **4,** 55–61, doi: 10.1038/ngeo1036.

Maeda, T., K. Obara, T. Furumura, and T. Saito (2011). Interference of long-period seismic wavefield observed by dense Hi-net array in Japan, *J. Geophys. Res.* **116,** no. B10303, doi: 10.1029/2011JB008464.

Nagaoka, Y., K. Nishida, Y. Aoki, and M. Takeo (2010). Temporal change of phase velocity beneath Mt. Asama, Japan, inferred from coda wave interferometry, *Geophys. Res. Lett.* **37,** L22311, doi: 10.1029/2010GL045289.

Nagaoka, Y., K. Nishida, Y. Aoki, M. Takeo, and T. Ohminato (2012). Seismic imaging of magma chamber beneath an active volcano, *Earth Planet. Sci. Lett.* **333/334,** 1–8, doi: 10.1016/j.epsl.2012.03.034.

Nishida, K., H. Kawakatsu, and K. Obara (2008). Three-dimensional crustal S wave velocity structure in Japan using microseismic data recorded by Hi-net tiltmeters, *J. Geophys. Res.* **113,** no. B10302, doi: 10.1029/2007JB005395.

Nishida, K., J.-P. Montagner, and H. Kawakatsu (2009). Global surface wave tomography using seismic hum, *Science* **326,** 112, doi: 10.1126/science.1176389.

Obara, K., K. Kasahara, S. Hori, and Y. Okada (2005). A densely distributed high-sensitivity seismograph network in Japan: Hi-net by National Research Institute for Earth Science and Disaster Prevention, *Rev. Sci. Instrum.* **76,** 021301, doi: 10.1063/1.1854197.

Peterson, J. (1993). Observations and modeling of seismic background noise, *U.S. Geol. Surv. Open-File Rept.* 93-322.

Shapiro, N. M., M. Campillo, L. Stehly, and M. H. Ritzwoller (2005). High-resolution surface-wave tomography from ambient seismic noise, *Science* **307,** 1615–1618, doi: 10.1126/science.1108339.

Takagi, R., H. Nakahara, T. Kono, and T. Okada (2014). Separating body and Rayleigh waves with cross terms of the cross-correlation tensor of ambient noise, *J. Geophys. Res.* **119,** 2005–2018, doi: 10.1002/2013JB010824.

van Wijk, K., D. Mikesell, T. Blum, M. Haney, and A. Calvert (2011). Estimating the Rayleigh-wave impulse response between seismic stations with the cross terms of the Green tensor, *Geophys. Res. Lett.* **38,** L16301, doi: 10.1029/2011GL047442.

APPENDIX

We show a theoretical basis for removing the coherent logger noise from a combination of ZR and RZ cross correlations. Consider two seismic stations, α and β, on the free surface: α is at the origin, and β is at distance r from the origin. In the frequency domain, vertical and radial motions, $u_{\alpha,Z}(0,f)$ and $u_{\alpha,R}(0,f)$, respectively, at station α are represented by the superposition of the plane Rayleigh waves and the coherent logger noise $E_\alpha(f)$ as

$$u_{\alpha,Z}(0,f) = \int_{-\pi}^{\pi} d\varphi A^R(\varphi,f) + D_{\alpha,Z}E_\alpha(f), \text{ and} \quad (A1)$$

$$u_{\alpha,R}(0,f) = \int_{-\pi}^{\pi} d\varphi i H^R(f) \cos\varphi A^R(\varphi,f)$$
$$+ (D_{\alpha,N}\cos\zeta + D_{\alpha,E}\sin\zeta)E_\alpha(f), \quad (A2)$$

and those at the station β are given by

$$u_{\beta,Z}(r,f) = \int_{-\pi}^{\pi} d\varphi A^R(\varphi,f)e^{ik^R r\cos\varphi} + D_{\beta,Z}E_\beta(f), \text{ and} \quad (A3)$$

$$u_{\beta,R}(r,f) = \int_{-\pi}^{\pi} d\varphi i H^R(f) \cos\varphi A^R(\varphi,f)e^{ik^R r\cos\varphi}$$
$$+ (D_{\beta,N}\cos\zeta + D_{\beta,E}\sin\zeta)E_\beta(f), \quad (A4)$$

in which f is the frequency, φ is the azimuth measured from a line connecting the two station, ζ is the azimuth of the two stations measured from the north, and $A^R(\varphi,f)$, $H^R(\varphi,f)$, and $k^R(f)$ represent the incident amplitude, the amplitude of the horizontal motion normalized by that of the vertical motion, and the wavenumber, respectively, of the Rayleigh wave. $D_{\alpha,Z}$, $D_{\alpha,N}$, and $D_{\alpha,E}$ represent the sensitivity of the digitizer for vertical, north–south, and east–west components, respectively, of station α; i in the radial component indicates a phase shift of $\pi/2$ between vertical and radial motions; and $\cos\varphi$ arises from the polarization of the Rayleigh wave. We assume that the coherent logger noise does not depend on the component of seismic records. We allow the coherent logger noise to have the dependence of stations because the coherent logger noise repeating every minute varies with the ambient noise amplitude. We ignore incoherent noise because it does not contribute to the cross spectrum as described in equation (2). Hereafter, the frequency dependence is omitted in the presentation.

Let us assume random uncorrelated waves as

$$\langle A^R(\varphi)^* A^R(\varphi') \rangle = \frac{\langle |A^R(\varphi)|^2 \rangle}{2\pi}\delta(\varphi - \varphi'), \quad (A5)$$

$$\langle A^R(\varphi)^* E_\alpha \rangle = 0, \text{ and} \quad (A6)$$

$$\langle A^R(\varphi)^* E_\beta \rangle = 0, \quad (A7)$$

in which $\langle\rangle$ indicates ensemble average. With this assumption, the ensemble average of cross spectra ϕ_{ZR} and ϕ_{RZ} can be written as

$$\phi_{ZR}(r) = \langle u_{\alpha,Z}(0)^* u_{\beta,R}(r) \rangle$$
$$= \frac{1}{2\pi}\int_{-\pi}^{\pi} d\varphi i H^R \cos\varphi \langle |A^R(\varphi)|^2 \rangle e^{ik^R r\cos\varphi}$$
$$+ D_{\alpha,Z}D_{\beta,R}\langle E_\alpha^* E_\beta \rangle, \text{ and} \quad (A8)$$

$$\phi_{RZ}(r) = \langle u_{\alpha,R}(0)^* u_{\beta,Z}(r) \rangle$$
$$= \frac{-1}{2\pi}\int_{-\pi}^{\pi} d\varphi i H^R \cos\varphi \langle |A^R(\varphi)|^2 \rangle e^{ik^R r\cos\varphi}$$
$$+ D_{\alpha,R}D_{\beta,Z}\langle E_\alpha^* E_\beta \rangle, \quad (A9)$$

in which $D_{\alpha,R} = D_{\alpha,N}\cos\zeta + D_{\alpha,E}\sin\zeta$ and $D_{\beta,R} = D_{\beta,N}\cos\zeta + D_{\beta,E}\sin\zeta$. In equations (A8) and (A9), the sign of the Rayleigh-wave term (the first term) is opposite, while that representing the coherent logger noise (the second term) is the same. Therefore, the difference of ZR and RZ correlations eliminates the power spectrum of the coherent logger noise by retaining the Rayleigh-wave term as

$$\frac{W_{RZ}\phi_{ZR}(r) - W_{ZR}\phi_{RZ}(r)}{W_{ZR} + W_{RZ}}$$
$$= \frac{1}{2\pi}\int_{-\pi}^{\pi} d\varphi iH^R \cos\varphi\langle|A^R(\varphi)|^2\rangle e^{ik^R r\cos\varphi}, \quad \text{(A10)}$$

in which $W_{ZR} = D_{\alpha,Z}D_{\beta,R}$ and $W_{RZ} = D_{\alpha,R}D_{\beta,Z}$ are weighting factors associated with the sensitivity of the digitizer at two stations. For isotropic incidence, $\langle|A^R(\varphi)|^2\rangle = a_0^R$ so that the cross spectrum is expressed by the first-order Bessel function of the first kind as

$$\frac{W_{RZ}\phi_{ZR}(r) - W_{ZR}\phi_{RZ}(r)}{W_{ZR} + W_{RZ}} = \frac{iH^R a_0^R}{2\pi}\int_{-\pi}^{\pi} d\varphi \cos\varphi e^{ik^R r\cos\varphi}$$
$$= -H^R a_0^R J_1(k^R r).$$
$$\text{(A11)}$$

Equation (A11) is identical to that given by Haney *et al.* (2012). If all components of the two stations have the same sensitivity of the digitizer, the left side of equations (A10) and (A11) is simplified as

$$\frac{W_{RZ}\phi_{ZR}(r) - W_{ZR}\phi_{RZ}(r)}{W_{ZR} + W_{RZ}} = \frac{\phi_{ZR}(r) - \phi_{RZ}(r)}{2}. \quad \text{(A12)}$$

For Hi-net data, because the difference of the sensitivity is small enough, we used equation (A12) in Figure 1e,f.

Ryota Takagi
Kiwamu Nishida
Yosuke Aoki
Takuto Maeda
Komei Masuda
Minoru Takeo
Kazushige Obara
Earthquake Research Institute
University of Tokyo
1-1 Yayoi 1, Bunkyo-ku
Tokyo 113-0032, Japan
yaoki@eri.u-tokyo.ac.jp

Katsuhiko Shiomi
National Research Institute for Earth Science and Disaster Prevention
3-1 Tennnodai
Tsukuba, Ibaraki 305-0006, Japan

Minemori Sato
Hakusan Corporation
1-1 Nikko-cho, Fuchu
Tokyo 183-0044, Japan

Kazuo Saito
Keisokugiken Corporation
2021-5 Hoshakuji, Takanezawa Town
Tochigi 329-1233, Japan